Journal of Power Sources 264 (2014) 83–91

Contents lists available at ScienceDirect

Journal of Power Sources

journal homepage: www.elsevier.com/locate/jpowsour

Full-ionic liquid gel electrolytes: Enhanced photovoltaic performances in dye-sensitized solar cells

Qinghua Li [a], Qunwei Tang [b,*], Benlin He [b], Peizhi Yang [c]

[a] Key Laboratory of Nondestructive, Ministry of Education, Nanchang Hangkong University, Nanchang 330063, Jiangxi Province, PR China
[b] Institute of Materials Science and Engineering, Ocean University of China, Qingdao 266100, Shandong Province, PR China
[c] Key Laboratory of Advanced Technique & Preparation for Renewable Energy Materials, Ministry of Education, Yunnan Normal University, Kunming 650092, PR China

HIGHLIGHTS

- Ionic liquid-imbibed gel electrolyte is synthesized to replace traditional liquid electrolyte.
- Nonvolatility of ionic liquid is expected to enhance the long-term stability of DSSCs.
- The ionic conductivity of ionic liquid-imbibed gel electrolyte is enhanced.
- The conversion efficiency of the quasi-solid-state DSSC is 7.19%.

GRAPHICAL ABSTRACT

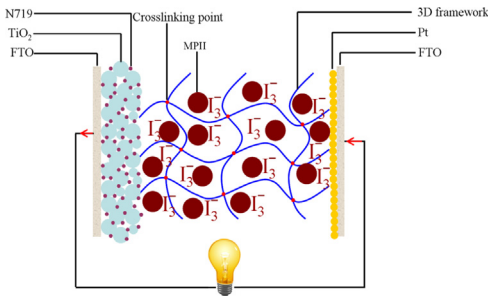

ARTICLE INFO

Article history:
Received 10 March 2014
Received in revised form
3 April 2014
Accepted 17 April 2014
Available online 28 April 2014

Keywords:
Ionic liquid
Gel electrolyte
Quasi-solid-state dye-sensitized solar cell
Three-dimensional framework
Amphiphilic hydrogel

ABSTRACT

Liquid electrolytes containing redox species have been widely used in dye-sensitized solar cells (DSSCs), whereas the volatility of organic solvents has been a tremendous obstacle for their commercial application. To assemble durable DSSCs, here we report the synthesis of full-ionic liquid electrolyte, in which 1-butyl-3-methylimidazolium nitrate is employed as solvent and 1-methyl-3-propylimidazolium iodide is iodide source. Using the imbibition performance of amphiphilic poly(acrylic acid/gelatin) [poly(AA/GR)] and poly(acrylic acid/cetyltrimethyl ammonium bromide) [poly(AA/CTAB)] matrices, full-ionic liquid electrolytes are imbibed into three-dimensional framework of poly(AA/GR) or poly(AA/CTAB) to form stable gel electrolytes. Room-temperature ionic conductivities as high as 17.82 and 18.44 mS cm^{-1} are recorded from full-ionic liquid imbibed poly(AA/GR) and poly(AA/CTAB) gel electrolytes, respectively. Promising power conversion efficiencies of 7.19% and 7.15% are determined from their DSSC devices in comparison with 6.55% and 6.12% from traditional acetonitrile-based poly(AA/GR) and poly(AA/CTAB) gel electrolytes, respectively. The new concept along with easy fabrication demonstrates the full-ionic liquid electrolytes to be good alternatives for robust gel electrolytes in quasi-solid-state DSSCs.

1. Introduction

Dye-sensitized solar cell (DSSC), an electrochemical device directly converting solar energy to electricity, has attracted growing interests because of their merits on relatively high power conversion efficiency, low fabrication cost, and environmental-friendliness [1–6]. A typical DSSC device is composed of a dye sensitized TiO_2 photoanode, a counter electrode, and redox electrolyte. The task of redox electrolyte is to regenerate excited dye molecules and to be subsequently reduced by the counter electrode. To obtain higher reaction kinetics, organic solvents such as

* Corresponding author. Tel./fax: +86 532 66781690.
E-mail address: tangqunwei@ouc.edu.cn (Q. Tang).

http://dx.doi.org/10.1016/j.jpowsour.2014.04.095
0378-7753/

acetonitrile are always employed as mediums for the transportation of iodide/triiodide (I^-/I_3^-) redox couples [7–10]. However, low ionic conductivity, insufficient penetration of the electrolyte into nanoporous structure of TiO_2 film, and volatility of organic solvents have been tremendous obstacles for the commercial application of DSSCs [11–13]. Therefore, it is a prerequisite to find an alternative solvent with nonvolatility, easy synthesis, low cost and environmental-friendly natures for I^-/I_3^- loading. By addressing these issues, room-temperature ionic liquids are preferred candidates.

Room-temperature ionic liquids, liquid state within temperature of 100 °C, are defined as ionic solvents composed of positively and negatively charged ions. They are always characterized with high glass transition temperature [14], reasonable thermal stability [15], high conductivity [16], and especially good dissolution to iodine and iodide [17]. Up to now, there are few reports on the employment of full-ionic liquid electrolyte in DSSCs, not to mention full-ionic liquid electrolyte imbibed three-dimensional (3D) amphiphilic framework-based quasi-solid-state DSSCs.

In the current work, 3D poly(acrylic acid/glycerol) [poly(AA/GR)] and poly(acrylic acid/cetyltrimethyl ammonium bromide) [poly(AA/CTAB)] polymer composites are employed as placeholders for full-ionic liquid loading to replace acetonitrile-contained iodide electrolytes [18,19]. Crosslinked poly(acrylic acid) is a typical 3D framework capable of absorbing enormous aqueous solution because of decoration with hydrophilic –COOH groups, however, modification of poly(acrylic acid) by glycerol (GR) or cetyltrimethyl ammonium bromide (CTAB) can generate amphiphilicity to poly(AA/GR) or poly(AA/CTAB). The imbibed full-ionic liquid electrolyte in 3D framework of poly(AA/GR) or poly(AA/CTAB) can not leak even during cell assembly and operation. The resultant gel electrolytes are subsequently assembled into quasi-solid-state DSSC devices, which are expected to be honored by long-term stability. The objectives of this study are the synthesis of full-ionic liquid imbibed poly(AA/GR) and poly(AA/CTAB) gel electrolytes and their characterizations as well as the photovoltaic performances of assembled DSSCs from the gel electrolytes.

2. Experimental

2.1. Materials

Unless noted otherwise, chemicals were purchased from Sigma–Aldrich and used as received.

2.2. Synthesis of 3D poly(AA/GR) matrix

Poly(AA/GR) matrix was synthesized by the procedures: 5 ml of GR and 10 g of acrylic acid (AA) were dispersed in 10 ml of deionized water. Subsequently, initiator potassium peroxydisulfate (KPS) (mass ratio of KPS to AA was 0.008) and crosslinker *N*,*N*′-methylene bisacrylamide (NMBA) (mass ratio of NMBA to AA was 0.0005) were added to the mixed solution. When the viscosity of the poly(AA/GR) prepolymers reached around 180 mPa s^{-1}, the reagent was poured into a petri dish and cooled to room temperature until the formation of an elastic gel. After rinsing with excess deionized water, the samples were vacuum dried at 80 °C. Finally, the sample was vacuum dried at 80 °C for more than 12 h.

2.3. Synthesis of 3D poly(AA/CTAB) matrix

Poly(AA/CTAB) matrix was synthesized by the procedures: 1 g of cetyltrimethyl ammonium bromide (CTAB) and 10 g of AA were dispersed in 10 ml of deionized water. Subsequently, initiator KPS (mass ratio of KPS to AA was 0.008) and crosslinker NMBA (mass ratio of NMBA to AA was 0.0005) were added to the mixed solution. When the viscosity of the poly(AA/CTAB) prepolymers reached around 180 mPa s^{-1}, the reagent was poured into a petri dish and cooled to room temperature until the formation of an elastic gel. After rinsing with excess deionized water, the samples were vacuum dried at 80 °C. Finally, the sample was vacuum dried at 80 °C for more than 12 h.

2.4. Synthesis of [AMIM]NO_3, [AMIM]BF_4, and MPII

The [AMIM]NO_3, [AMIM]BF_4, and 1-methyl-3-propylimidazolium iodide (MPII) were synthesized by following steps [20,21]: A mixture of 23.0 g of *N*-methyl-imidazolium and 25.3 g of allyl nitrate was vigorously agitated in a three-necked flask equipped with mechanical stirrer and thermometer. The excess allyl nitrate was removed by keeping temperature at 60–65 °C for 6–7 h, while the surplus *N*-methyl-imidazolium was extracted by vacuum drying at 80 °C for 48 h to obtain a transparently viscous liquid. 35.0 g of the as-synthesized viscous liquid, 20.0 g of silver nitrate, and 50.0 ml of methanol were mixed in another three-necked flask at 40 °C for 48 h to obtain [AMIM]NO_3. The unreacted sodium bicarbonate and methanol were removed in filtering and evaporating processes.

A mixture of 23.0 g of *N*-methyl-imidazolium and 25.3 g of allyl nitrate was vigorously agitated in a three-necked flask equipped with mechanical stirrer and thermometer. The excess allyl nitrate was removed by keeping temperature at 60–65 °C for 6–7 h, while the surplus *N*-methyl-imidazolium was extracted by vacuum drying at 80 °C for 48 h to obtain a transparently viscous liquid. 35.0 g of the as-synthesized viscous liquid, 20.0 g of $AgBF_4$, and 50.0 ml of methanol were mixed in another three-necked flask at 40 °C for 48 h to obtain [AMIM]BF_4. The unreacted sodium bicarbonate and methanol were removed in filtering and evaporating processes.

Methyl imidazole and iodopropane with a molar ratio of 1: 1.1 were mixed in a 250 ml neck boiling flask which was sealed by toluene. The mixture was deaerated by bubbling N_2 for 5 min and dark-agitated at 35 °C for 24 h. Resultant product was thoroughly rinsed with anhydrous ether and shaken for 20 min and then kept stilling for 1 h until the liquid became brownish red. After rotary evaporation at 30 °C for 3 h, final MPII can be obtained.

2.5. Fabrication of full-ionic liquid imbibed gel electrolytes

Full-ionic liquid imbibed poly(AA/GR) gel electrolyte was prepared according to the following procedures [22–25]: 0.2 g of poly(AA/GR) was immersed in an ionic liquid electrolyte solution at ambient temperature, resulting in the diffusion of full-ionic liquid electrolyte into poly(AA/GR) framework and formation of a swollen sample to reach absorption saturation. The ionic liquid electrolyte consisted of 0.5 M I_2, 0.01 M LiI in mixed organic solvent of 40 vol% MPII, 50 vol% [AMIM]NO_3, and 10 vol% *N*-methyl pyrrolidone. Ionic liquid imbibed poly(AA/CTAB) gel electrolyte was prepared according to the following procedures: 0.2 g of poly(AA/CTAB) was immersed in an IL electrolyte solution at ambient temperature, resulting in the diffusion of RTIL electrolyte into the poly(AA/CTAB) network and formation of a swollen sample to reach absorption saturation. The RTIL electrolyte consisted of 0.5 M I_2, 0.01 M LiI in mixed organic solvent of 40 vol% MPII, 50 vol% [AMIM]BF_4, and 10 vol% *N*-methyl pyrrolidone.

The ionic liquid loading could be calculated according to the following equation:

$$\text{Ionic liquid loading}\left(\text{g g}^{-1}\right) = \frac{W_t - W_d}{W_d} \quad (1)$$

where W_t (g) and W_0 (g) were the masses of full-ionic liquid imbibed gel electrolyte and pure matrix, respectively.

2.6. Assembly of quasi-solid-state DSSCs

A layer of TiO_2 nanocrystal anode film with a thickness of 10 μm and active area of 0.09 cm^2 was prepared by coating the TiO_2 colloid using a doctor blade technique, followed by sintering in air at 450 °C for 30 min. Subsequently, the TiO_2 film was soaked in a 0.3 mM N719 [cis-di(thiocyanato)-*N*,*N*′-bis(2,2′-bipyridyl-4-carboxylic acid-4-tetrabutylammonium carboxylate, purchased from Solaronix, SA, Switzerland] ethanol solution for 24 h to uptake N719 dye for the fabrication of dye-sensitized TiO_2 photoanode. The quasi-solid-state DSSC from full-ionic liquid imbibed poly(AA/GR) or poly(AA/CTAB) gel electrolyte at an imbibition equilibrium was fabricated by sandwiching a slice of gel electrolyte with a thickness of around 1 mm between dye-sensitized TiO_2 anode and a Pt counter electrode (300–400 μm in thickness, purchased from Dalian HepatChroma SolarTech Co., Ltd.).

2.7. Photovoltaic measurements

The photocurrent–voltage (*J*–*V*) curves of the assembled quasi-solid-state DSSCs were recorded on an Electrochemical Workstation (Xe Lamp Oriel Sol^{3}A™ Class AAA Solar Simulators 94023A, USA) under irradiation of a simulated solar light from a 100 W xenon arc lamp in ambient atmosphere. The incident light intensity was 100 mW cm^{-2} (AM 1.5) which was calibrated using a FZ-A type radiometer (purchased from Beijing Normal University Photoelectric Instrument Factory). Each DSSC device was measured at least five times to eliminate experimental error and a compromise *J*–*V* curve was employed.

2.8. Characterizations

The morphologies of the gel electrolytes were captured with a Zeiss Ultra plus field emission scanning electron microscopy (FESEM). To observe the internal 3D microstructure, swollen gel electrolytes were first cut into ultrathin film, followed by the loading into a chamber under freezing temperature and high vacuum to remove solvent. The ^{1}HNMR spectra were recorded on a Bruker Advance-400 spectrometer with d-chloroform as the solvent and tetramethylsilane as the internal standard. Fourier transform infrared spectrometry (FTIR) spectra were recorded on a Vertex 70 FTIR spectrometer (Bruker). The ionic conductivity of gel-electrolyte was measured by using a pocket conductivity meter (HANNA8733, Hanna Instruments). Thermogravimetric analyses (TGA) were conducted on a TA Instruments Model SDT Q600 thermogravimetric analyzer. The samples were heated at a heating rate of 10 °C min and atmospheric pressure, and under N_2 flow (90 mL min^{-1}). The weight loss as a function of temperature was recorded continuously in the range of 25–590 °C. Preliminary tests, small masses (20–25 mg) of each material, thinly distributed in the crucible. The ionic conductivity of gel-electrolyte was measured by using a pocket conductivity meter (HANNA8733, Hanna Instruments). The instrument was calibrated with 0.01 M KCl aqueous solution prior to experiments. Tafel-polarization curves of the symmetrical cells fabricated of samples were measured by CHI660D electrochemical workstation. The symmetrical dummy cells fabricated with two identical Pt electrodes (Pt electrode/gel electrolyte/Pt electrode). The electrochemical impedance spectroscopy (EIS) was carried out using a CHI660E electrochemical workstation at a constant temperature of 20 °C with an ac signal amplitude of 20 mV in the frequency range from 0.1 to 10^5 Hz at a 10 V dc bias in the dark. The porosity was analyzed by an AutoPore IV9500 mercury porosimeter (Micromeritics, USA) in a pressure range of 0.5–30,000 psia.

3. Results and discussion

3.1. Morphology observation

The cross-sectional SEM images of pure poly(AA/GR) and poly(AA/CTAB) matrices are shown in Fig. 1, which suggests well-interconnected and microporous frameworks capable of caging enormous full-ionic liquid electrolyte in the microporous structure because of high porosity [68.8% and 67.4% for microporous poly(AA/GR) and poly(AA/CTAB), respectively]. The absorbed full-ionic liquid electrolyte is expected to be sealed in the 3D frameworks [26–28]. The formation of 3D frameworks of poly(AA/GR) and poly(AA/CTAB) matrices is a typical free radical process. Complex monomers from AA/GR or AA/CTAB are formed by the hydrogen-bonding between AA (C═O) and GR (-OH) or electrostatic attraction of AA (negatively charged) and CTAB (positively charged) during the mixing process. For the polymerization, thermal cleavage of initiator KPS can initiate the complex monomers and crosslinker NMBA to generate radicals. During the complicated polymerization process, a 3D framework can be formed because of the macrobiradicals nature of NMBA [18,19,29,30]. In fact, the pore size and porosity can be controlled by adjusting synthesis conditions, such as initiator dosage, crosslinker dosage, reaction temperature, concentration of AA monomer, and mass ratio of AA to GR or mass ratio of AA to CTAB. The matrix framework with higher porosity can provide higher ionic liquid loading in per unit volume of gel electrolyte, therefore, the transfer ability of gel electrolyte toward I^-/I_3^- redox couples is further enhanced. The increased charge-transfer capacity can accelerate the recovery of excited dyes and redox reaction between $I^- \leftrightarrow I_3^-$, which is favorable to elevating photocurrent density and fill factor of DSSC device. The focus of the current work was to display the feasibility of employing amphiphilic poly(AA/GR) or poly(AA/CTAB) gel material as a placeholder to fabricate robust gel electrolyte and therefore efficient DSSC device.

3.2. Structural analysis

^{1}HNMR spectrum of [AMIM]NO_3 was provided to confirm its molecular structure. Fig. 2a gives δ values of 5.4, 6.0, and 4.8, revealing the hydrogen atom positions in (1)–(3). The hydrogen atom at position (4) can be confirmed by detecting δ value of 3.9, whereas the single peak at $\delta = 7.5$ is a coupling reflection of hydrogen atoms posited at (5) and (6), and $\delta = 8.7$ is attributed to D_2O. Till now, we can make a conclusion that the chemical structure of [AMIM]NO_3 is in the inset of Fig. 2a. The ^{1}HNMR spectrum of [AMIM]BF_4 is provided in Fig. 2b, giving δ values of 5.0, 6.2, and 5.6, revealing the hydrogen atom positions in (1)–(3). The hydrogen atom at position (4) can be confirmed by detecting δ value of 4.0, whereas the single peak at $\delta = 7.6$ is a coupling reflection of hydrogen atoms posited at (5) and (6), and $\delta = 8.8$ is attributed to D_2O. Till now, we can make a conclusion that the chemical structure of [AMIM]BF_4. Fig. 2c shows the ^{1}HNMR spectrum of MPII, giving δ values of 1.0, 2.1, and 4.3 which are attributed to the hydrogen atoms at position (1), (2), and (3) in *n*-propyl, respectively. Hydrogen atom at position (4) gives a δ of 4.1, and coupling of (5) & (6) atoms shows a single peak at $\delta = 7.7$, whereas peak at $\delta = 4.8$ is attributed to D_2O and hydrogen atom at position (7) gives a peak at $\delta = 4.8$. Fig. 2d gives the FTIR spectrum of resultant MPII, showing absorption bands at 2960, 2870, 1572, 1172, 1432, 954, and 3170 cm^{-1} which can be attributed to C–H stretching in $-CH_3$ group, C–H stretching in $-CH_2$ group, C═N stretching in imidazole

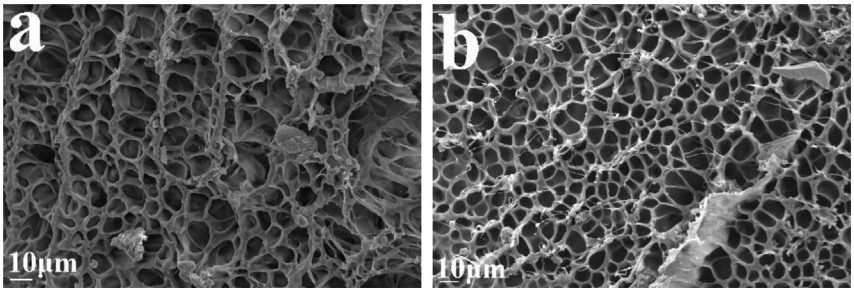

Fig. 1. SEM photographs of (a) pure poly(AA/GR) and (b) poly(AA/CTAB) matrices.

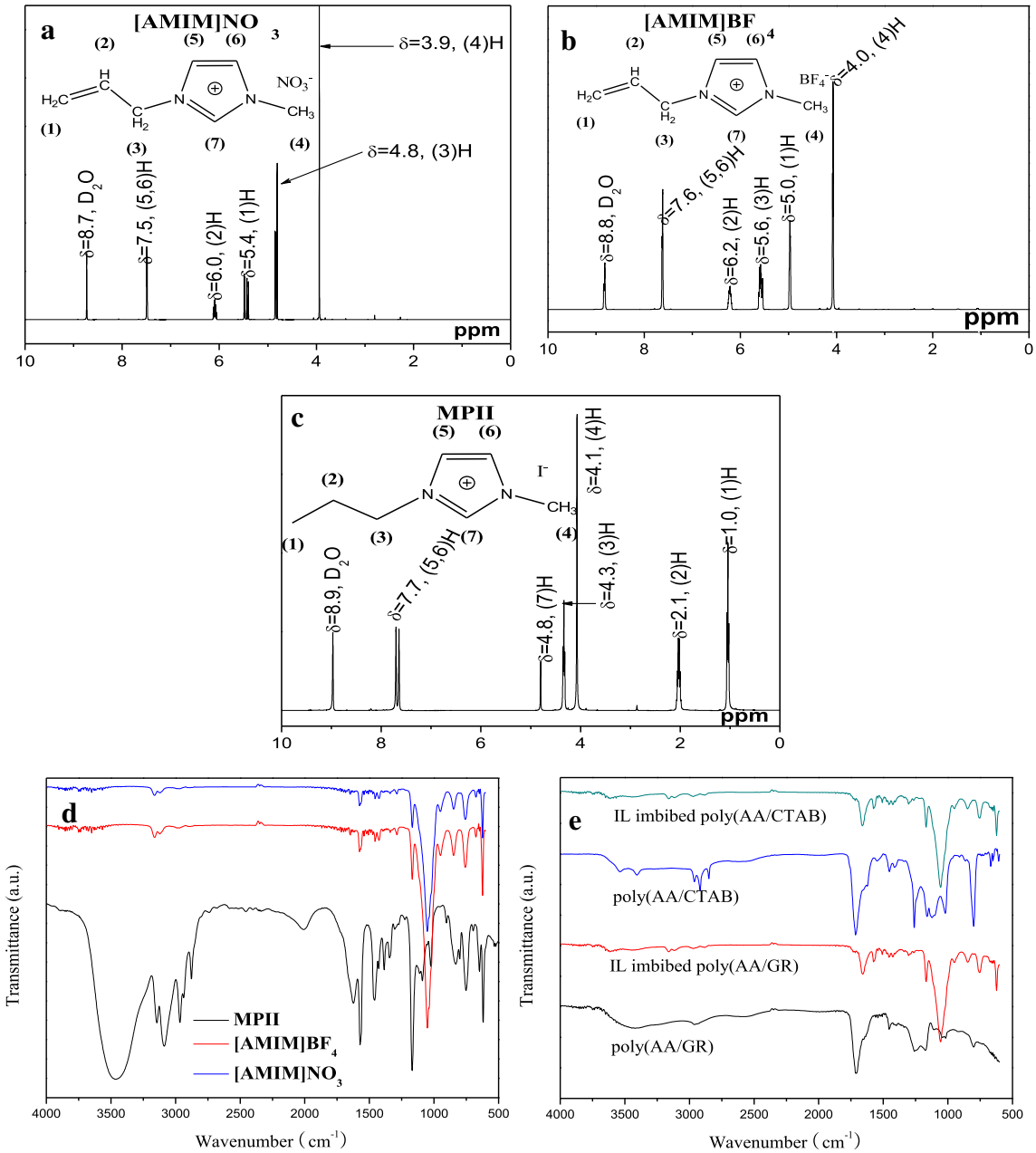

Fig. 2. ^{1}HNMR spectra of (a) [AMIM]NO_3, (b) [AMIM]BF_4, and (c) MPII, and FTIR spectra of (d) [AMIM]NO_3, [AMIM]BF_4, and MPII, and (e) pure poly(AA/GR) matrix, full-ionic liquid imbibed poly(AA/GR), pure(AA/CTAB), and full-ionic liquid imbibed poly(AA/CTAB). If not special specified, "IL" in the figure represents "full-ionic liquid".

ring, C–H bending in imidazole ring, C–H bending in side $-CH_2$ group, stretching of imidazole ring, and O–H in H_2O, respectively. By combining ^{1}HNMR and FTIR spectra, we can confirm that inset in Fig. 2c is the molecular structure of MPII. All the absorption bands of [AMIM]NO_3, [AMIM]BF_4, and MPII can be detected in IL imbibed poly(AA/GR) or poly(AA/CTAB) electrolyte (Fig. 2e), indicating that the ILs have been incorporated into the 3D framework of poly(AA/GR) or poly(AA/CTAB) gel.

3.3. Thermal analysis

The thermal analysis behaviors of pure poly(AA/GR) and pure poly(AA/CTAB) matrices are shown in Fig. 3. The main thermal degradation of matrix under nitrogen atmosphere occurs in a narrow temperature region between 350 and 450 °C. However, the imbibition of IL electrolyte into 3D framework of poly(AA/GR) or poly(AA/CTAB) results in a decreased thermal stability, giving a decomposition temperature region between 300 and 400 °C because of the poor thermal performance of room-temperature ILs. It is noteworthy to mention that the weight losses of pure poly(AA/GR) or poly(AA/CTAB) matrix and IL imbibed poly(AA/GR) or poly(AA/CTAB) electrolyte within 100 °C are nearly the same, indicating that the IL can be well-sealed in the 3D frameworks of gel matrices. The good thermal stability and good ionic liquid retention along with easy synthesis demonstrates the IL imbibed gel electrolyte to be good candidate in quasi-solid-state DSSC devices.

3.4. Ionic conductivity

The ionic liquid loading and ionic conductivity of the IL imbibed poly(AA/GR) gel electrolyte are shown in Fig. 4a. The highest ionic liquid loading of 8.03 g g^{-1} and an ionic conductivity of 17.82 mS cm^{-1} are recorded at an imbibition time of 18 days, which are higher than that from acetonitrile-contained poly(AA/GR) [23]. The measured ionic conductivity from gel electrolyte is close to 18.72 mS cm^{-1} from pure IL electrolyte, indicating that the 3D framework provides facile channels for rapid charge transfer. The increased liquid electrolyte dosage in per unit volume of gel electrolyte and ionic transfer ability are expected to have an acceleration effect on power conversion efficiency of the quasi-solid-state DSSCs. The imbibition kinetics of dense poly(AA/GR) matrix in IL electrolyte, shown in inset of Fig. 4a, is mainly due to the Flory theory from osmotic pressure across the poly(AA/GR) matrix. The loading of IL electrolyte increases with elongation of swelling time, indicating a stepwise diffusion of IL electrolyte into 3D framework of poly(AA/GR). The absorption equilibrium can be obtained at swelling time of around 17 days, and no further diffusion occurs under longer immersion time. Similar trend is also detected from IL imbibed poly(AA/CTAB) gel electrolyte (Fig. 4c), in which the highest IL electrolyte loading and ionic conductivity are 13.66 g g^{-1} and 18.44 mS cm^{-1}, respectively. In order to determine the loading of IL electrolyte by poly(AA/GR) or poly(AA/CTAB), the accumulative IL electrolyte loading over time have been fitted using the Fickian theory [24].

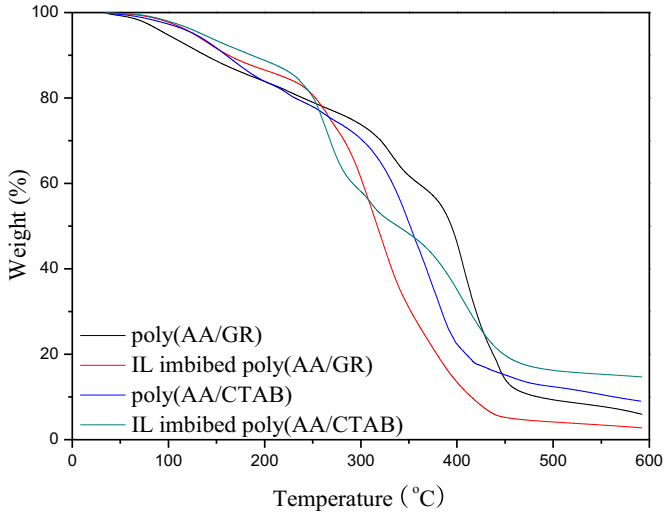

Fig. 3. TGA curves of pure poly(AA/GR), full-ionic liquid imbibed poly(AA/GR), pure poly(AA/CTAB), and full-ionic liquid imbibed poly(AA/CTAB).

$$\frac{M_t}{M_\infty} = kt^n \tag{2}$$

where M_t and M_∞ are the masses of the loaded IL electrolyte at time t and at equilibrium, respectively. k is a characteristic rate constant relating to the properties of poly(AA/GR) or poly(AA/CTAB), and n is a transport number characterizing the transport mechanism. $n \leq 0.5$ suggests a Fickian or Case I transport behavior in which the poly(AA/GR) or poly(AA/CTAB) framework relaxation is much faster than the diffusion; $n = 1$ gives a non-Fickian or Case II mode of transport where IL electrolyte uptake is controlled by diffusion process. $0.5 < n < 1$ refers to an anomalous or a Case III mode in which structural relaxation is comparable to diffusion. By plotting $\log(M_t/M_\infty)$ vs $\log(t)$, the n value are calculated as 0.60 and 0.63 for poly(AA/GR) and poly(AA/CTAB), respectively, indicating an anomalous mechanism mode in which structural relaxation is comparable to diffusion.

The conductivity–temperature (σ–T) relationships for the IL imbibed poly(AA/GR) and poly(AA/CTAB) gel electrolytes at various imbibition time are shown in Fig. 4b and d, respectively. From the figures, one can find that the conductivity increases with elevation of temperature and the $\ln(\sigma)$ versus $1/T$ plots is almost linear, which is in a good agreement with previous results [22,23,25,31].

The elevation of ionic conductivity with temperature is assigned to enhancement of ions transportation. The data can be better fitted by Arrhenius equation:

$$\sigma(T) = A\exp\left(\frac{-E_a}{k_B T}\right) \tag{3}$$

where A is a constant, E_a is the activation energy, k_B is Boltzmann's constant, and T is the absolute temperature. According to Fig. 4b and Equation (3), the E_a values for the IL imbibed poly(AA/GR) gel electrolyte are calculated as 22.06 kJ mol^{-1} (1 day), 18.36 kJ mol^{-1} (4 days), 17.18 kJ mol^{-1} (7 days), 14.44 kJ mol^{-1} (10 days), 10.21 kJ mol^{-1} (13 days), and 9.67 kJ mol^{-1} (17 days). However, the E_a for the IL imbibed poly(AA/CTAB) gel electrolyte are calculated as 21.84 kJ mol^{-1} (1 day), 19.28 kJ mol^{-1} (5 days), 16.18 kJ mol^{-1} (10 days), 13.86 kJ mol^{-1} (15 days), 10.95 kJ mol^{-1} (20 days), and 8.97 kJ mol^{-1} (22 days). Low E_a value in gel electrolyte suggests a facile ionic transport along conducting channels. It is reasonable that the conducting channels tend to be interconnecting at higher imbibition aging because of gradual diffusion and rearrangement of IL within 3D poly(AA/GR) or poly(AA/CTAB) framework. Therefore, the interconnected micropores of poly(AA/GR) or poly(AA/CTAB) framework provides superhighway for facile ion transport. There is a consensus that the ionic conductivity is determined by the thermal hopping frequency in the case of an ionic transport process involving intermolecular ion hopping, resulting in proportional relationship to $\exp(-E_a/K_bT)$ and therefore leading to an Arrhenius conductivity–temperature relationship [32]. The ion hopping

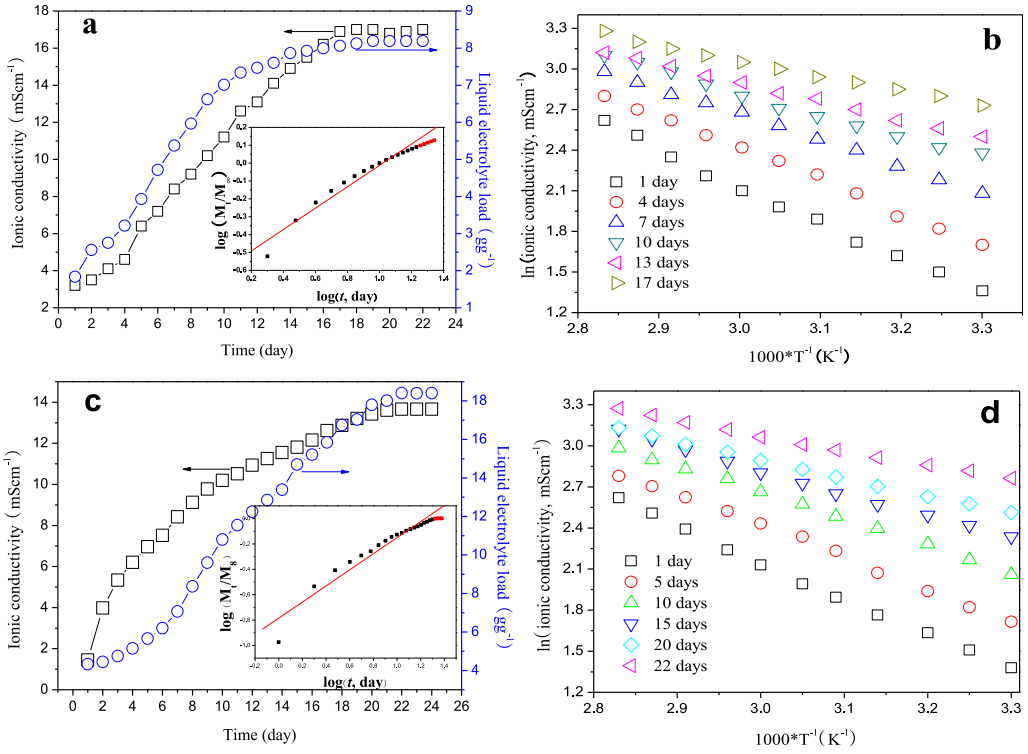

Fig. 4. Dependence of ionic liquid-based gel electrolyte loading and ionic conductivity on imbibition time: (a) poly(AA/GR) and (c) poly(AA/CTAB). The inset shows the imbibition kinetics of poly(AA/GR) or poly(AA/CTAB) toward full-ionic liquid electrolyte. Dependence of ionic conductivity on temperature at different imbibition time: (b) poly(AA/GR) and (d) poly(AA/CTAB).

kinetics and ionic conductivity are expected to be significantly enhanced at higher imbibition aging.

3.5. Electrochemical behaviors of the gel electrolytes

As a powerful tool to explore the electrochemical process, EIS has been widely employed in testing the electrocatalytic activity for the regeneration of redox species. For EIS experiments, the Pt/gel electrolyte/Pt is contained in a symmetric cell composed of a gel electrolyte sandwiched by two FTO supported Pt glass electrodes. Fig. 5a shows the Nyquist plots of Pt/gel electrolyte/Pt devices using the four electrolytes. Typically, the intercept on the real axis (high frequency) can be attributed to the series resistance (R_s) between counter electrode and the gel electrolyte. The first semicircle (middle frequency) can be assigned to the resistance capacitance networks of the electrode/electrolyte interface, including the charge transfer resistance (R_{ct}). The EIS curves are shown in Fig. 5a and the data are summarized in Table 1. In the current research, the R_{ct} values of IL imbibed poly(AA/GR) gel electrolyte and acetonitrile-contained poly(AA/GR) gel electrolyte are 7.55 and 13.57 Ω cm^2, respectively. Similarly, the R_{ct} values of IL imbibed and acetonitrile-contained poly(AA/CTAB) gel electrolytes are 9.07 and 9.31 Ω cm^2, respectively. Compared with acetonitrile-contained poly(AA/GR) and poly(AA/CTAB), the decreased R_{ct} of IL imbibed poly(AA/GR) and poly(AA/CTAB) may be the result of enhancement of ionic conductivity in the resultant IL electrolyte than that of acetonitrile-contained liquid electrolyte. Lower R_{ct} in IL imbibed poly(AA/GR) or poly(AA/CTAB) gel electrolyte reveals that the charge-transfer ability at IL imbibed gel electrolyte/Pt interface is higher than that in acetonitrile-contained gel electrolyte/Pt

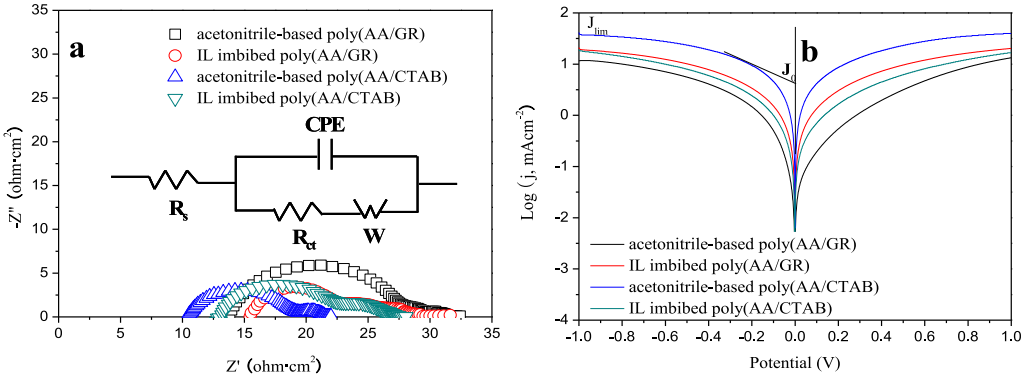

Fig. 5. (a) Nyquist plots and (b) Tafel-polarization curves of acetonitrile-contained iodide imbibed poly(AA/GR), acetonitrile-contained iodide imbibed poly(AA/CTAB), full-ionic liquid imbibed poly(AA/GR), and full-ionic liquid imbibed poly(AA/CTAB) gel electrolytes. Inset is a related equivalent circuit diagram.

Table 1
The photovoltaic performances of the quasi-solid-state DSSC based on different electrolytes.

Gel electrolytes	R_s (Ω cm^2)	R_{ct} (Ω cm^2)	V_{oc} (V)	J_{sc} (mA cm^{-2})	*FF*	η (%)
Acetonitrile-contained iodide imbibed poly(AA/GR)	13.84	13.57	0.708	13.60	0.68	6.55
Full-ionic liquid imbibed poly(AA/GR)	15.36	7.55	0.730	14.27	0.69	7.19
Acetonitrile-contained iodide imbibed poly(AA/CTAB)	10.73	9.31	0.751	13.58	0.60	6.12
Full-ionic liquid imbibed poly(AA/CTAB)	12.95	9.07	0.750	14.44	0.66	7.15
Full-ionic liquid	–	–	0.731	14.14	0.70	7.27

interface. The rapid transport of refluxed electrons from Pt counter electrode to gel electrolyte is expected to accelerate the reduction reaction of iodides.

Tafel-polarization measurements are used to reconfirm the electrocatalytic activity of the gel electrolytes, which is also performed with the dummy cells similar to those used in EIS measurements, as shown in Fig. 5b. A larger slope in the anodic or cathodic branch indicates a higher exchange current density (J_0) on the electrode. J_0 can be also calculated by Equation (4) [33]:

$$J_0 = \frac{RT}{nFR_{ct}} \quad (4)$$

Apparently, the calculated J_0 also follows the order of IL imbibed poly(AA/GR) or poly(AA/CTAB) gel electrolyte > acetonitrile-contained poly(AA/GR) or poly(AA/CTAB) gel electrolyte, suggesting that IL imbibed poly(AA/GR) electrolyte shows a superior electrocatalytic activity for triiodides reduction, which is consistent with the J_{sc} order. In addition, the Tafel polarization curves contain the information about limiting current density (J_{lim}), which can be expressed as:

$$J_{lim} = \frac{2neD_cN_A}{l} \quad (5)$$

The IL imbibed poly(AA/GR) or poly(AA/CTAB) electrolyte shows a high limiting diffusion current density (J_{lim}) relative to that of pure poly(AA/GR) or poly(AA/CTAB), reflecting a higher diffusion velocity for the redox couple in the electrolyte. In theory, J_0 varies inversely with R_{ct}. With the EIS results, the change tendency of J_0 for various electrodes is generally in accordance with those presented in the Tafel curve plots. J_{lim} is determined by the diffusion properties of the redox couple and the counter electrodes; At the same potential, a large J_{lim} indicates a large diffusion coefficient and a small Z_W [34,35]. The J_{lim} value of IL imbibed poly(AA/GR) or poly(AA/CTAB) gel electrolyte is higher than that of acetonitrile-contained gel electrolyte. Consequently, we can make a conclude from the electrochemical and EIS results that IL imbibed poly(AA/GR) or poly(AA/CTAB) gel electrolyte has a higher electrocatalytic activity than acetonitrile-contained gel electrolyte. The order of electrocatalytic activity well explains the order of J_{sc} [36,37].

3.6. Photovoltaic behaviors of the quasi-solid-state DSSCs

The photocurrent versus photovoltage (*J–V*) curves of quasi-solid-state DSSCs from various gel electrolytes are shown in Fig. 6a. As a reference, the *J–V* curve of the DSSC employing IL is also recorded under one sun illumination. The IL electrolyte contains: 0.5 M I_2, 0.01 M LiI, 40 vol% MPII, 50 vol% [AMIM]NO_3, and 10 vol% *N*-methyl pyrrolidone. The acetonitrile-contained liquid electrolyte contains: 0.1 M LiI, 0.01 M I_2, 20 vol% NMP and 80 vol% acetonitrile. Under a simulated solar light irradiation with intensity of 100 mW cm^{-2}, the photoelectric parameters of DSSCs such as short circuit current density (J_{sc}), open circuit voltage (V_{oc}), fill factor (*FF*) and energy conversion efficiency (η) are summarized in Table 1. It is evident that nearly all photoelectric parameters of the quasi-solid-state DSSC from IL imbibed poly(AA/GR) or poly(AA/CTAB) gel electrolyte are higher than that from traditional gel electrolyte. J_{sc} is dependent on the electron density on conduction band of TiO_2, whereas the photogenerated electrons are injected from excited dyes. The maximum V_{oc} is determined by the difference between the quasi Fermi energy of electrons in TiO_2 and redox potential energy of electrolyte [38]. However, the real V_{oc} of a DSSC is generally smaller than this theoretical limit, and one of the reasons is a backward reaction between electrons and redox electrolyte [39]. From the dark *J–V* characteristics, as shown in Fig. 6b, it is apparent that the DSSCs employing IL imbibed poly(AA/CTAB) and acetonitrile-based poly(AA/CTAB) gel electrolytes have the smallest dark current density at the same voltage. The dark current density in DSSC device is attributed to the triiodides combination with electrons on CB of TiO_2 at the TiO_2/electrolyte interface. The smaller dark current density indicates that the reduction of triiodides on the TiO_2/electrolyte interface is retarded. This is a key factor for the highest V_{oc} from IL imbibed poly(AA/CTAB) and acetonitrile-based poly(AA/CTAB) gel electrolytes based DSSCs. Interestingly, the DSSC from IL imbibed poly(AA/GR) gel electrolyte has larger dark current but lower R_{ct} than that from IL imbibed poly(AA/CTAB). Generally, a larger R_{ct} means a facile transportation of I^-/I_3^- redox species within 3D framework of matrix. However, the porosity of poly(AA/GR) (68.8%) is larger than 67.4% for poly(AA/CTAB),

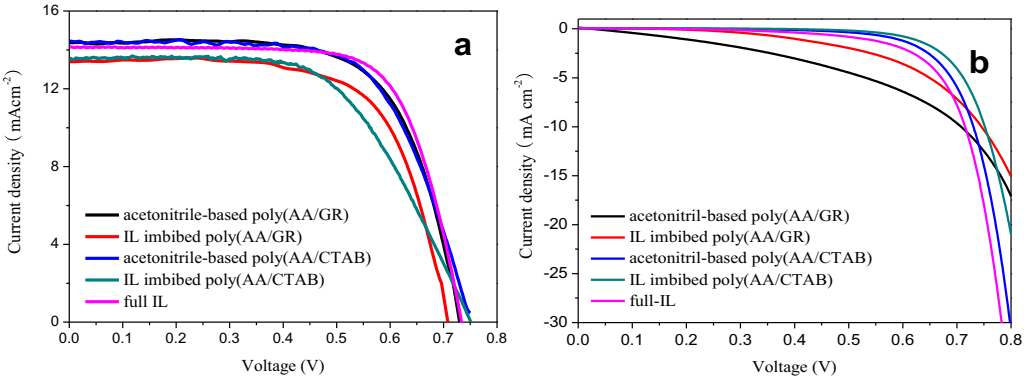

Fig. 6. Characteristic photocurrent–voltage (*J–V*) curves of quasi-solid-state DSSCs from acetonitrile-contained iodide imbibed poly(AA/GR), acetonitrile-contained iodide imbibed poly(AA/CTAB), full-ionic liquid imbibed poly(AA/GR), full-ionic liquid imbibed poly(AA/CTAB) gel electrolytes, and full-ionic liquid: (a) under one sun illumination; (b) in the dark.

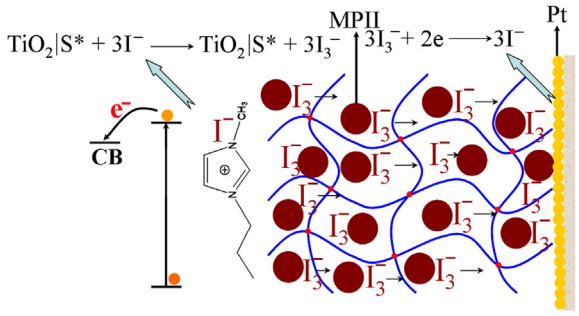

Fig. 7. Schematic illustration on the quani-solid-state DSSC from full-ionic liquid imbibed gel electrolyte.

yielding an increased contact rate of triiodides with photo-generated electrons.

It has been known that the IL imbibed poly(AA/GR) or poly(AA/CTAB) has an increased charge-transfer ability. Once the excited dyes release electrons, iodide ions participate in their regeneration and change into triiodides, as shown in Fig. 7. Therefore, the enhancement in R_{ct} can accelerate the reaction kinetics of dye recovery and therefore the electron density on conduction band of TiO_2. Moreover, the *FF* is also a parameter relating to the charge-transfer ability of electrolyte material. The DSSCs employing IL imbibed poly(AA/GR) and poly(AA/CTAB) display power conversion efficiencies of 7.19% and 7.15% from their quasi-solid-state DSSCs in comparison with 6.55% and 6.12% from traditional acetonitrile-contained poly(AA/GR) and poly(AA/CTAB) gel electrolytes, respectively. Although the efficiencies from IL imbibed poly(AA/GR) and poly(AA/CTAB) based DSSCs are lightly lower than 7.27% from IL based DSSC, the retention of IL has been significantly enhanced. To reveal the potential mechanism of conversion efficiency, it is believed as a comprehensive effect of ionic conductivity of gel electrolyte, retention of solvent, and charge-transfer ability at gel electrolyte/Pt counter electrode interface. From the results, we can conclude that all of these performances have been enhanced in IL imbibed poly(AA/GR) or poly(AA/CTAB) gel electrolyte in comparison with that of acetonitrile-contained liquid electrolyte imbibed ones.

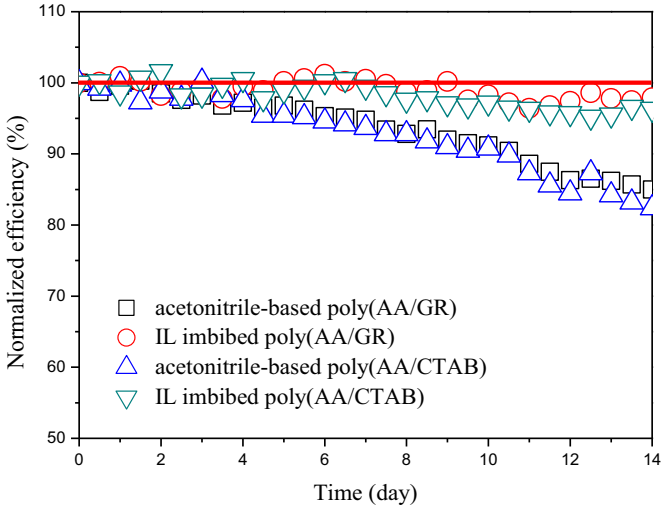

Fig. 8. Normalized power conversion efficiencies of DSSCs from acetonitrile-based liquid electrolyte-imbibed and ionic liquid-imbibed poly(AA/GR) and poly(AA/CTAB) gel electrolytes.

Fig. 8 shows the normalized power conversion efficiencies of DSSCs from IL imbibed poly(AA/GR) and poly(AA/CTAB) gel electrolytes, as a comparison, the results from acetonitrile-based liquid electrolyte-imbibed poly(AA/GR) and poly(AA/CTAB) electrolyte are also provided. After a work over 14 days, nearly 97% efficiencies are remained in the DSSCs from ionic liquid-based gel electrolytes, whereas that is only 83% for traditional acetonitrile-based ones because of the volatilization of organic solvent from 3D poly(AA/GR) or poly(AA/CTAB) framework. The volatilization of acetonitrile is expected to lose the medium for ionic transfer within gel electrolyte, therefore, the excited dye molecules can not be recovered by redox couples. Until now, we can make a conclusion that the DSSCs from IL imbibed poly(AA/GR) and poly(AA/CTAB) gel electrolytes have a reasonable durability.

4. Conclusions

In summary, iodide-containing room-temperature ILs have been successfully synthesized and imbibed into 3D frameworks of amphiphilic poly(AA/GR) and poly(AA/CTAB) matrices to form a durable gel electrolytes. Ionic conductivities of 17.82 and 18.44 mS cm^{-1} are recorded from IL imbibed poly(AA/GR) and poly(AA/CTAB), respectively. The quasi-solid-state DSSCs have promising power conversion efficiencies of 7.19% and 7.15% employing IL imbibed poly(AA/GR) and poly(AA/CTAB) gel electrolytes, respectively, which are higher than 6.55% and 6.12% of the DSSCs from acetonitrile-contained poly(AA/GR) and poly(AA/CTAB) gel electrolytes. Moreover, the DSSCs from IL imbibed poly(AA/GR) and poly(AA/CTAB) gel electrolytes have a good stability that from traditional acetonitrile-based gel electrolytes. This research opens a gateway to improve the photovoltaic performances of DSSCs and highlights competitive capacity of the quasi-solid-state DSSCs among photovoltaic devices.

Acknowledgments

The authors gratefully acknowledge the financial support of the National Natural Science Foundation of China (61366003, U1037604), The Science and Technology Project of the Education Department of Jiangxi Province, China (GJJ13474), Fundamental Research Funds for the Central Universities (201313001, 201312005), Shandong Province Outstanding Youth Scientist Foundation Plan (BS2013CL015), Doctoral Fund of Ministry of Education of China (20130132120023), Shandong Provincial Natural Science Foundation (ZR2011BQ017), and Research Project for the Application Foundation in Qingdao (13-1-4-198-jch).

References

[1] B. O'Regan, M. Grätzel, Nature 353 (1991) 737–740.
[2] U. Bach, D. Lupo, P. Comte, J.E. Moser, F. Weissortel, J. Salbeck, et al., Nature 395 (1998) 583–585.
[3] M. Grätzel, Nature 414 (2001) 338–344.
[4] Y. Hua, S. Chang, H. Wang, D. Huang, J. Zhao, T. Chen, et al., J. Power Sources 243 (2013) 253–259.
[5] J. Zhang, S. Li, H. Ding, Q. Li, B. Wang, X. Wang, H. Wang, J. Power Sources 247 (2014) 807–8012.
[6] J. Yu, J. Fan, B. Cheng, J. Power Sources 196 (2011) 7891–7898.
[7] H. Chen, Y. Chiang, C. Kung, N. Sakai, M. Ikegami, Y. Yamauchi, et al., J. Power Sources 245 (2014) 411–417.
[8] J. Chen, T. Peng, W. Shi, R. Li, J. Xia, Electrochim. Acta 107 (2013) 231–237.
[9] N. Jeon, D. Hwang, Y. Kang, S. Im, D. Kim, Electrochem. Commun. 34 (2013) 1–4.
[10] F. Matteocci, G. Mincuzzi, F. Giordano, A. Capasso, E. Artuso, C. Barolo, et al., Org. Electron. 14 (2013) 1882–1890.
[11] S. Nakade, T. Kanzaki, Y. Wada, S. Yanagida, Langmuir 21 (2005) 10803–10807.
[12] J. Freitas, A.F. Nogueira, M. Paoli, J. Mater. Chem. 19 (2009) 5279–5294.
[13] A. Nogueira, C. Longo, M. Paoli, Coord. Chem. Rev. 248 (2004) 1455–1468.

[14] J. Pitawala, M.A. Navarra, B. Scrosati, P. Jacobsson, A. Matic, J. Power Sources 245 (2014) 830–835.
[15] Q.W. Tang, Y. Li, Z.Y. Tang, J.H. Wu, J.M. Lin, M.L. Huang, J. Mater. Chem. 21 (2011) 16010–16017.
[16] Q.W. Tang, J.H. Wu, Z.Y. Tang, Y. Li, J.M. Lin, J. Mater. Chem. 22 (2012) 15836–15844.
[17] S.T. Fei, S.H.A. Lee, S.M. Pursel, J. Basham, A. Hess, C.A. Grimes, et al., J. Power Sources 196 (2011) 5223–5230.
[18] Q. Li, X. Chen, Q. Tang, H. Xu, B. He, Y. Qin, J. Mater. Chem. A 1 (2013) 8055–8060.
[19] Q. Li, Q. Tang, L. Lin, X. Chen, H. Chen, L. Chu, et al., J. Power Sources 245 (2014) 468–474.
[20] V. Jovanovski, B. Orel, I. Jerman, S.B. Hočevar, B. Ogorevc, Electrochem. Commun. 9 (2007) 2062–2066.
[21] Z. Zhang, Y. Wu, Q. Ge, S. Sun, C. Shi, Sol. Energy 84 (2010) 390–393.
[22] J. Wu, Z. Lan, J. Lin, Adv. Mater. 19 (2007) 4006–4011.
[23] Q. Li, J. Wu, Z. Tang, Y. Xiao, M. Huang, J. Lin, Electrochim. Acta 55 (2010) 2777–2781.
[24] N.W. Franson, N.A. Peppas, J. Appl. Polym. Sci. 28 (1983) 1299.
[25] J. Wu, S. Hao, Z. Lan, J. Am. Chem. Soc. 130 (2008) 11568–11569.
[26] S.S. Yuan, Q.W. Tang, B.L. He, Y. Zhao, J. Power Sources 260 (2014) 225–232.
[27] S.S. Yuan, Q.W. Tang, B.L. He, P.Z. Yang, J. Power Sources 254 (2014) 98–105.
[28] S.S. Yuan, Q.W. Tang, B.B. Hu, C.Q. Ma, J.L. Duan, B.L. He, J. Mater. Chem. A 2 (2014) 2814–2821.
[29] Z.Y. Tang, J.H. Wu, Q. Liu, M. Zheng, Q.W. Tang, Z. Lan, et al., J. Power Sources 203 (2012) 282–287.
[30] Z.Y. Tang, Q. Liu, Q.W. Tang, J.H. Wu, J.L. Wang, S.H. Chen, et al., Electrochim. Acta 58 (2011) 52–57.
[31] J. Wu, S. Hao, Z. Lan, J. Lin, M. Huang, Y. Huang, et al., Adv. Funct. Mater. 17 (2007) 2645–2652.
[32] A. Agrios, A. Hagfeldt, J. Phys. Chem. C 112 (2008) 10021–10026.
[33] B.L. He, Q.W. Tang, J.H. Luo, Q.H. Li, X.X. Chen, H.Y. Cai, J. Power Sources 256 (2014) 170–177.
[34] Y.D. Wang, M.X. Wu, X. Lin, Z.C. Shi, A. Hagfeldt, T.L. Ma, J. Mater. Chem. 22 (2012) 22155–22159.
[35] F. Gong, H. Wang, X. Xu, G. Zhou, Z. Wang, J. Am. Chem. Soc. 134 (2012) 10953–10958.
[36] J.D. Roy-Mayhew, D.J. Bozym, C. Punckt, I.A. Aksay, ACS Nano 4 (2010) 6203–6211.
[37] A. Hanch, A. Georg, Electrochim. Acta 46 (2001) 3457–3466.
[38] D. Cahen, G. Hodes, M. Grätzel, J.F. Guillemoles, I. Riess, J. Phys. Chem. B 164 (2000) 2053–2059.
[39] H.S. Jung, J.K. Lee, J. Phys. Chem. Lett. 4 (2013) 1682–1693.